Droplet formation by pressure-driven flow in T and X-junction microfluidic devices

Aaron Delahanty
BSc Mechanical Engineering

School of Engineering

College of Science and Engineering

University of Glasgow

Submitted in fulfillment of the requirements for the Degree of

Master of Science

2016

Abstract

Microfluidic devices generally require precise control of fluid flowrates in order to accurately and reliably perform their various functions. In the case of droplet-makers fluid flow may be manipulated to dictate the size, frequency and distribution of droplets. Multiple approaches may be taken in order to control fluid flow in such devices. Here a pressure-driven flow controller (PDFC) is developed and characterized for use as a flow provider for droplet-makers and as a tool for further microfluidics-based research.

Previously, droplet-makers that utilize volumetric flow control have been used to define the relationship between continuous and discontinuous phase flowrates and the resulting droplet parameters and flow regimes. Here pressure-driven droplet-makers are characterized and compared to the existing systems. Furthermore, an investigation into the ability to control droplet formation in real-time is conducted by quantifying the time-to-stability of the electronic flow controller and droplet-maker system.

The work conducted and presented here can be divided clearly into three sections (i) design, fabrication, development of the PDFC (ii) characterization of the PDFC system and (iii) investigation into the behavior of droplet-maker devices as driven by pneumatic pressure.

The PDFC system consists of a micro controller, sensing pressure transducers, regulating pressure transducers, as well as various pneumatic and electronic components used to integrate the system into University of Glasgow's Franke Lab's existing microfluidic test set-up. The system was characterized to show pressure control ranging from 0 to 1000mbar with 4 discreetly controlled channels capable of precision of XX with a time response of XX. When applied as the flow controller for droplet-makers it was found that droplet formation as defined by length:width behaved similarly to previously volumetric flow rate systems.

A major limitation of pressure-driven flow systems is that the flow rate within microfluidic devices varies as a function of device geometry. Herein significant discussion is presented as to methods of theoretical and experimental approximations of the volumetric flowrates resulting from pressure-driven flow.

Contents

List of Figures

Chapter 1

Introduction

Lorem ipsum dolor sit amet, consectetur adipiscing elit, sed do eiusmod tempor incididunt ut labore et dolore magna aliqua. Ut enim ad minim veniam, quis nostrud exercitation ullamco laboris nisi ut aliquip ex ea commodo consequat. Duis aute irure dolor in reprehenderit in voluptate velit esse cillum dolore eu fugiat nulla pariatur. Excepteur sint occaecat cupidatat non proident, sunt in culpa qui officia deserunt mollit anim id est laborum.

Chapter 2

Background Theory

Development of a pneumatic pressure driven flow system for use in microfluidic research requires a firm grasp on the transition from 'macro' fluidics to microfluidics. The system operates across a great range of scales drawing and compressing air from a room of several cubic meters that is subsequently used to provide flow in channels of only a few micrometers. Following the flow path of the system - compressed air is filtered and directed via large diameter ($5mm$) tubing to reagent columns of large diameter ($2cm$), where the compressed air acts on the reagent to produce flow through smaller tubing ($< 1mm$) before finally transitioning into the microfluidic device where channel dimensions are on the order of magnitude of micrometers. This range of scale is illustrated in Figure 2.1

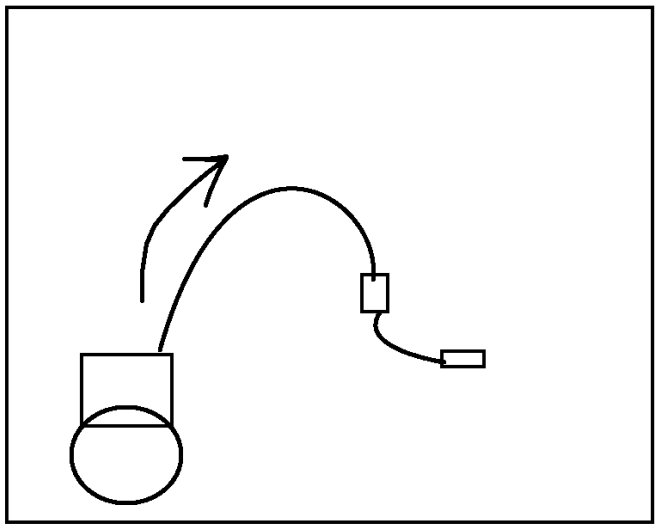

Figure 2.1: Illustration of the scales involved in the system.

The importance of forces that act on fluids therefore dramatically changes from the macro- to the microscale. With downscaling, the buoyancy, gravitational and inertial forces are less and less important and viscous and interfacial forces become more and more predominant.[13]

2.1 Droplet microfluidics Overview

Phase is a distinct state of matter in a system; matter that is identical in chemical composition and physical state and separated from other material by the phase boundary. Multiphase fluids are those in which there exist at least two different fluids in a system with different chemical composi- tions ? liquid/liquid, or with different physical states ? gas/ liquid.[13]. Here we neglect consideration of gas-liquid two phase systems.

[15, 12, 16]

The study of fluid dynamics requires the analysis of individual fluid forces (such as gravity, inertial, viscous, and interfacial forces) and an understanding of how these forces combine to define fluid behavior. In order to understand the transition from large dimension ($> 1mm$) to small dimension ($< 1mm$) systems it may be useful to understand how these forces relate to system dimensions by the way of scaling laws. Some fluid forces such as inertial forces and gravity forces are dependent on the *volume* of fluid involved. Other fluid forces are intrinsically defined by the *surface area* of the fluids such as viscous forces and interfacial forces. More broadly speaking each of various fluid forces may be dependent on the different orders of characteristic length, l. For example, inertial force is dependent on density, ρ, which may be expressed as mass per volume or mass per l^3, as shown in Equation 2.1. Similarly, interfacial tension is often defined as the partial differential of the Gibb's free energy over area, where the area term may be expressed in terms of l^2, shown in Equation 2.2.

$$i = \rho\nu^2 = \frac{m}{V}\nu^2 = \frac{m}{(l^3)}\nu^2 \tag{2.1}$$

$$\gamma = \frac{\partial G}{\partial A} = \frac{\partial G}{\partial (l^2)} \tag{2.2}$$

Consider the relative effect these individual forces have on the overall fluid behavior in which the volume dependent forces have an l^3 term and the surface forces have a l^2 term, as shown in Equation 2.3 on the next page [3]

$$\frac{SurfaceForces}{VolumeForces} \propto \frac{l^2}{l^3} = l^{-1} \lim_{l \to 0} \to \infty \tag{2.3}$$

From this comes the realization that as systems are miniaturized towards a theoretical zero-dimension the surface forces begin play an exponentially larger effect relative to the volume forces, illustrated in Figure 2.2.

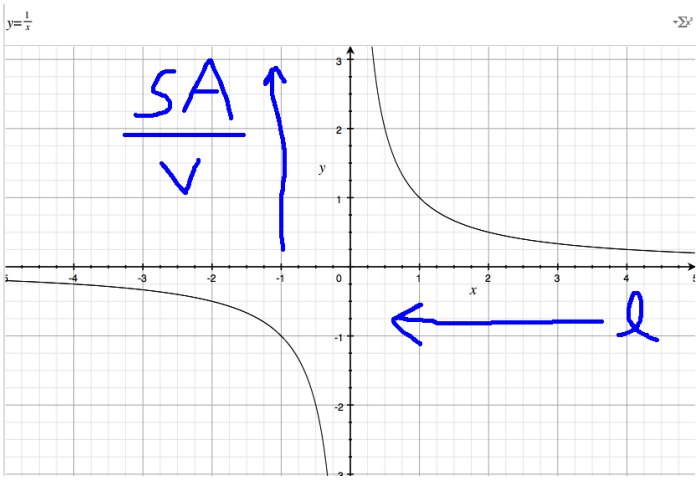

Figure 2.2: Illustration of the law of scales as fluid systems are miniaturized.

Navier-Stokes Early attempts at approximating fluid flow by Bernoulli and his pupil Euler completely neglected the viscosity term (an aforementioned surface force) in their mathematical expressions. In systems of small dimensions the viscosity effects are dominant and these approximations are inadequate. The Navier-Stokes expression accommodates viscous forces and is essentially a statement of force balance between inertial, pressure and viscous forces, shown in Equation . In most microfluidic systems the inertial forces are small enough that they may be neglected and the expression reduces to the statement that the net pressure forces are equal to the negative net viscous forces [11].

$$\rho\left(\frac{\partial \nu}{\partial t} + \nu \cdot \nabla \nu\right) = -\nabla P + f + \eta \nabla^2 \nu + \nabla \sigma \tag{2.4}$$

$$\frac{\partial \nu}{\partial t} + \nabla \cdot (\rho \nu) = 0 \tag{2.5}$$

$$\rho \frac{\partial \nu}{\partial t} = -\nabla P + f + \eta \nabla^2 \nu + \nabla \sigma \tag{2.6}$$

âbove equations from [13]

Dimensionless Groups In many cases fluid flow at the microscale can be best categorized by comparing *dimensionless groups* driven by fluid parameters such as viscosity, velocity, density and system geometry, as is the case of the dimensionless group known as Reynold's Number *(Re)* shown in Equation 2.7 . Regardless of the specific fluid or geometric parameters, systems with similar *Re* numbers general behave similarly - making it powerful tool in characterization of a microfluidic system. The *Re* value can be described in real world terms as a relation between the inertial forces and viscosity forces at play in a system. At the microscale viscous forces are dominant over inertial forces thus the *Re* value is typically very low, indicating flow is laminar [9].

$$Re = \frac{\rho \nu L}{\mu} \tag{2.7}$$

Where ρ is fluid density, ν is fluid velocity, L is characteristic length, and μ is fluid viscosity. The *Re* value dictates whether the system will be within the laminar or turbulent regime. *Re* values tend to be small (< 5) for microfluidic systems because the spatial scale, and therefore characteristic length, are small while fluid viscosity is constant relative to larger-scale systems [4]. As the majority of microfluidic systems feature small *Re* numbers the dimensionless group becomes less valuable in the differentiation and categorization of different systems.

For water in a straight micro- or nanochannel with a diameter between 100 nm and 100 ?m, where ?(H2O)=1.02510? 3 Pa s, ?(H2O)=103 kg m? 3 and v=1 mm s?1, the calculated Reynolds number lies between 10? 1 and 10? 4. For a gas, oxygen for instance, ?(O2)= 20.31710? 6 Pa s and ?(O2)=1.429 kg m? 3, the Reynolds number in the same system ranges from 10?5 to 10?2. Therefore, inertial forces are overwhelmed by interfacial forces in microfluidic devices, and laminar flow is expected in micro- and nanochannels, and not turbulent or random flow[13].

Other dimensionless groups such as Capillary Number, Peclet Number, Viscosity Ratios, Flowrate Ratios are commonly used to describe microfluidic systems - specifically droplet-producing geometries such as the device inestigater in section 'asdafs'. [7]

The Capillary number *(Ca)* is a dimensionless group that compares the relative contribution of interfacial forces and viscous forces. The capillary number is especially useful in discussion of two-phase microfluidic systems because it neglects any inertial forces and is capable of describing droplet formation behavior as influenced by solution viscosity and surface energies. The *Ca* is defined as shown in Equation 2.8 on the following page [4].

$$Ca = \frac{\mu u}{\gamma} \tag{2.8}$$

Where μ is defined as the viscosity of the continuous phase, u is the mean fluid velocity, and γ is the interfacial tension between the discontinuous and continuous phases. The viscous forces and interfacial forces determining fluid behavior are generally understood to act tangentially and normal to the two-phase interface, respectively. Viscous forces along the droplet surface work in elongation of surface of the droplet where as interfacial forces work to minimize the interfacial are. These two opposing behaviors when acting in different ratios dictate the droplet behavior as categorized by the different fluid regimes dripping, squeezing, jetting(XX?)[13].

Two stable droplet formation regimes exist (i) *dripping* - in which the viscous forces associated with the continuous phase flow are significantly large to cause shearing of the immiscible thread and the production of a droplet prior to blocking the outlet channel and (ii) *squeezing* - in which the immiscible thread blocks the majority of the outlet channel prior to collapse and droplets are formed by a squeezing effect due to the pressure build up caused by the blocked channel.

2.2 Hydrodynamic Resistance

$\Delta P = R_{HYD} Q$

$Q_1 = Q_2 = Q_3 = Q_4$

$R_{HYD} = R_1 + R_2 + R_3$

$R_1 = R_3 = \frac{8\eta L}{\pi r^4}$

$R_2 = \frac{28.4\eta L}{h^4}$

For the purpose of quantifying the contribution to total pressure drop of the droplet-maker relative to the inlet and outlet tubing the following values were applied to first solve for the flowrate at an arbitray pressure of 500mbar. Assuming that P_4 is equivalent to atmospheric pressure, 0 Pa, and $L_1 = 0.100m$, $L_2 = 0.001m$, $n = 1cP = 0.001Pa - s$, $r = 0.0025m$ and $h = 0.000030m$. Take $P_1 = 500mbar = 50kPa$ which is mid operational range for the system.

$R_1 = R_3 = \frac{8(0.001)(0.100)}{\pi 0.0025^4} = 6.52 \times 10^6 \frac{kg}{m^4 s}$

$R_2 = \frac{28.4(0.001)(0.001)}{0.000030^4} = 3.51 \times 10^{13} \frac{kg}{m^4 s}$

Clearly the resistance seen over the length of the simplified droplet-maker is several orders of magnitude greater than the resistance of the input/output lines. The total pressure $(P_4 - P_1)$ is known (it is the command pressure of the PDFC) and the

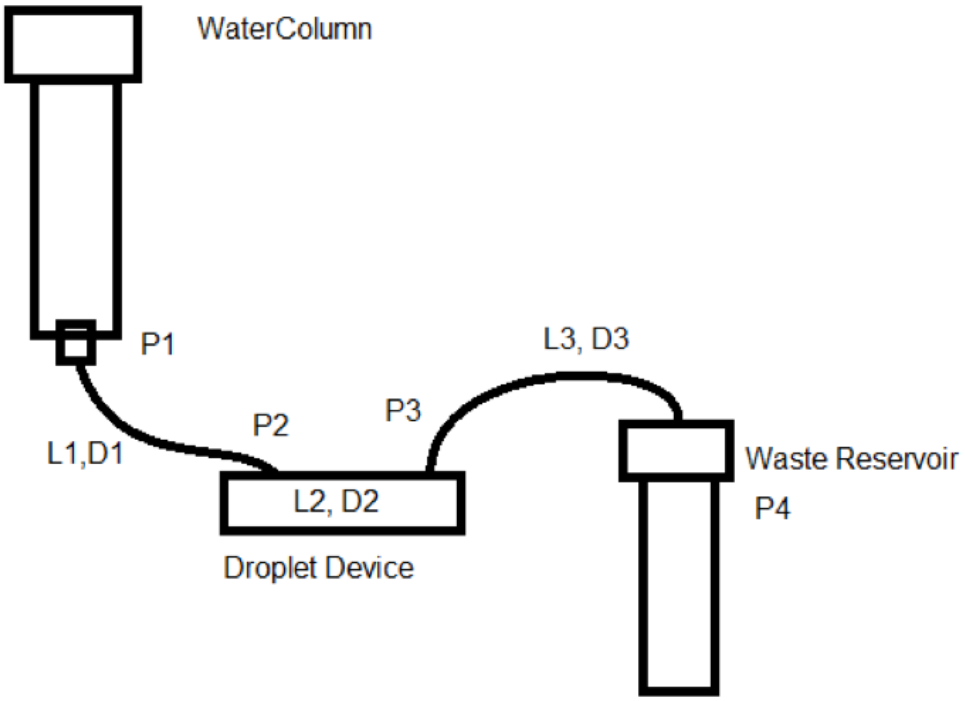

Figure 2.3: The microfluidic system detailed from the reagent water column to the waste reservoir.

individual pressure differentials can be calculated as follows:

$$P_4 - P_1 = (2(\frac{8\eta L_1}{\pi r^4}) + \frac{28.4\eta L_2}{h^4})Q$$

First solving for the flowrate:

$$Q = \frac{P_4 - P_1}{(2(\frac{8\eta L_1}{\pi r^4}) + \frac{28.4\eta L_2}{h^4})}$$

$$Q = \frac{50{,}000}{(2(6.52*10^6)+3.51*10^{13})} = 1.42 \times 10^{-9}\frac{m^3}{s}$$

$$Q = 1.42 * 10^{-9}\frac{m^3}{s} \times \frac{1000L}{m^3} = 1.42 \times 10^{-6}\frac{L}{s}$$

Assuming that the system is at steady state and therefore the microfluidic structure (tubing and PDMS) is not expanding due to internal pressure we can infer that by conservation of mass and assumed incompressible fluids that the volumetric flowrate is constant across each of the system pressure points shown in Figure 2.3. We can then produce the following system of equations:

$P_2 - P_1 = (R_1)Q$

$P_3 - P_2 = (R_2)Q$
$P_4 - P_3 = (R_3)Q$
Applying the previously calculated resistances and flowrate the following pressure differentials are obtained:
$P_2 - P_1 = 9.26 \times 10^{-3} \frac{kg}{m \cdot s^2} = 9.26 \times 10^{-3} Pa$
$P_3 - P_2 = 49.84 \times 10^{3} \frac{kg}{m \cdot s^2} = 49.84 \times 10^{3} Pa$
$P_4 - P_3 = 9.26 \times 10^{-3} \frac{kg}{m \cdot s^2} = 9.26 \times 10^{-3} Pa$

At these values (and given these are all simple linear equations this should be the case regardless of flow viscosity, etc.) the pressure drop across the micro-scale device comprises of:
$\frac{P_3 - P_2}{P_4 - P_1} = \frac{49.84 \times 10^3}{50.00 \times 10^3} = 0.9968$
And so it may be appropriate to neglect the pressure drops across the tubing and assume that the PDFC applied pressure is equivalent to the pressure applied across the droplet-maker. This can be further justified by the fact that the control precision of the system (a few mbar) is larger than the negligible pressure differentials of the tubing sections. XX consider modeling this using the same modeling software used for the BD lab (especially modeling the pressure drops across the microfluidic device itself.

Chapter 3

System Development

3.1 Design

3.2 Characterization

Note on time response: "The major drawback of passive control is the slow response time in the order of seconds or even minutes.32 The long response time comes from the relatively large fluidic resistance of the tubing and the fluidic capacitance caused by the compressibility of the liquid or the channel material.33,34"[5]

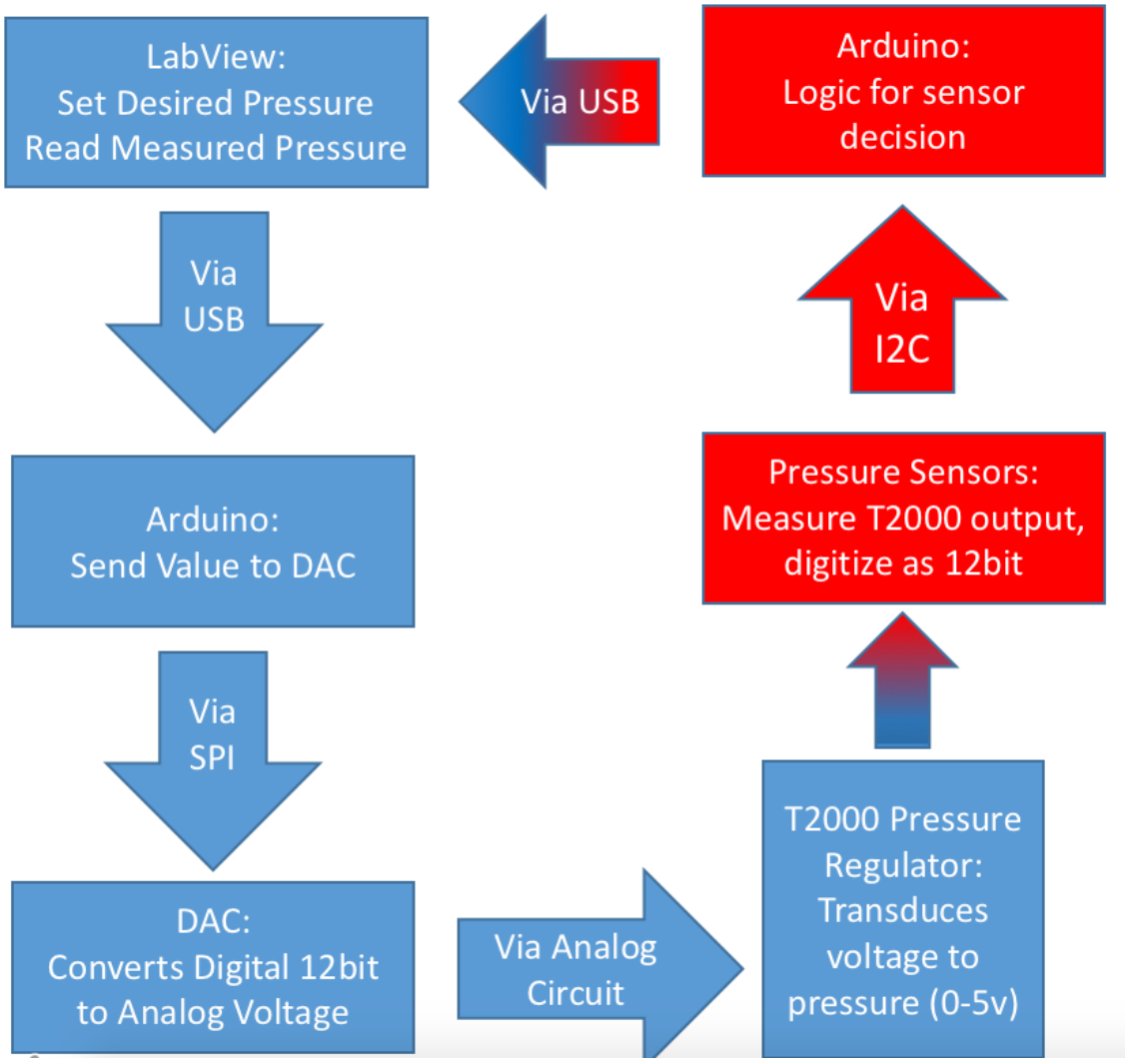

Figure 3.1: The control loop used to set and measure channel pressures using the PDFC

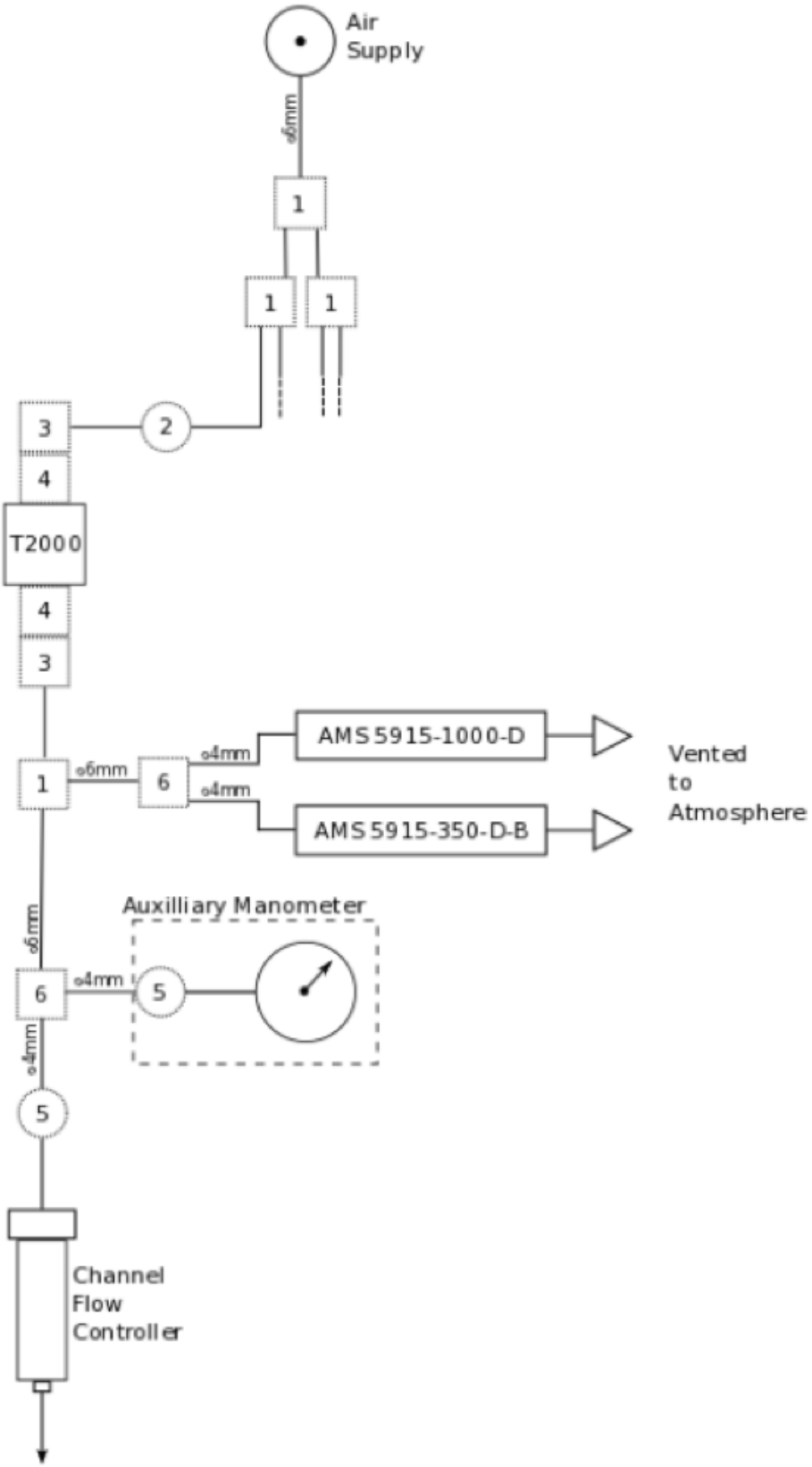

Figure 3.2: The pneumatic schematic detailing a single channel of the PDFC

Chapter 4

System Application - Droplet Microluidics

4.1 Aims

The application of the PDFC to droplet microfluidics serves two purposes. First, it verifies that the system is functioning as intended for use as a research tool. Second, it allows the characterization of droplet formation by a pressure driven flow in conjunction with X and T-junction geometry, an area currently underdeveloped [6]. These aims can be fulfilled by the following two objectives:

1. Determine how applied pressure determine droplet formation regime
2. Relate applied pressure to droplet scaling law [16]

4.2 Methods

4.2.1 Device Generation

4.2.2 Experimental Procedure

Droplet formation was captured on a high speed camera at 2.5k to 20k frames per second. The applied control pressure was held constant for the continuous phase at a nominal value of 40, 60 and 80 mbar while varying the discontinuous phase control pressure. Discontinuous phase control pressure was varied at intervals of ≈5mbar until droplet formation ceased due to the onset of backflow or instability, for low or high pressures, respectively. The captured images were then analyzed using a custom imageJ script to determine droplet length, L, and position, X, along an arbitrarily defined axis parallel to the geometry's outlet channel.

4.3 Results

For the T-junction channel geometry described the dimensionless droplet ratio of droplet length, L, over channel width, W, is plotted as a function of the applied control pressure ratios, $\frac{P_{H_2O}}{P_Oil}$, shown in Figure 4.1. Error bars have been calculated by standard deviation of measured droplet length which results in error equal to or smaller than the symbol size and thus not shown.

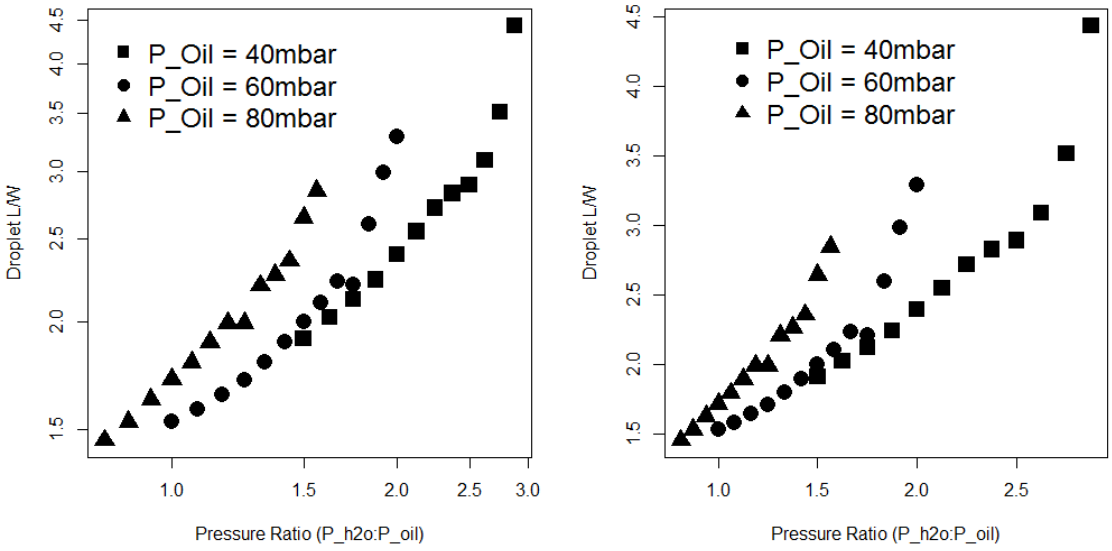

Figure 4.1: Log-log (left) and linear(right) plots of droplet length as a function of the applied control pressure ratio for T-junction geometry.

Outer Ca values are calculated given an interfacial tension of $\gamma = 2.87 \times 10^{-3} \frac{N}{m}$, continuous phase viscosity of $\mu = 1.24 \times 10^{-3} Pa \cdot s$[1], and mean velocity, u, as determined by droplet position over consecutive frames as shown in Equation 4.1.

$$[u] = \left[\frac{pixels}{frames}\right]\left[\frac{frames}{sec}\right]\left[\frac{meters}{pixel}\right] = \left[\frac{meters}{sec}\right] \tag{4.1}$$

Droplet length is plotted as a function of capillary number as shown in Figure 4.2 on the following page for each of the applied continuous pressures. Images of droplet formation are shown within the squeezing and dripping regimes for each control pressure. The image shown was captured one frame prior to droplet formation.

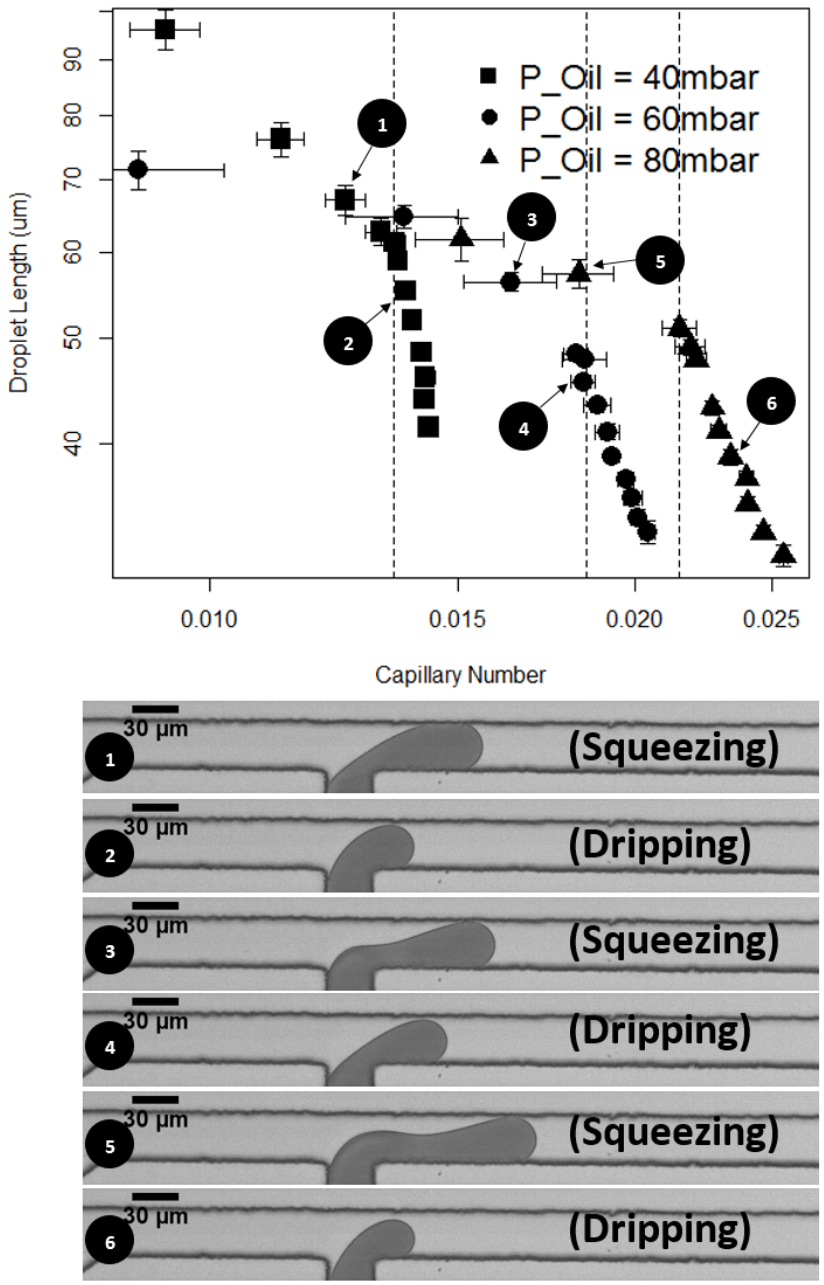

Figure 4.2: Top: Droplet length as a function of Capillary number across squeezing and dripping regimes, the transition between dripping and squeezing regimes is marked by vertical dashed lines. Bottom: Typical images of droplet elongation just prior to formation.

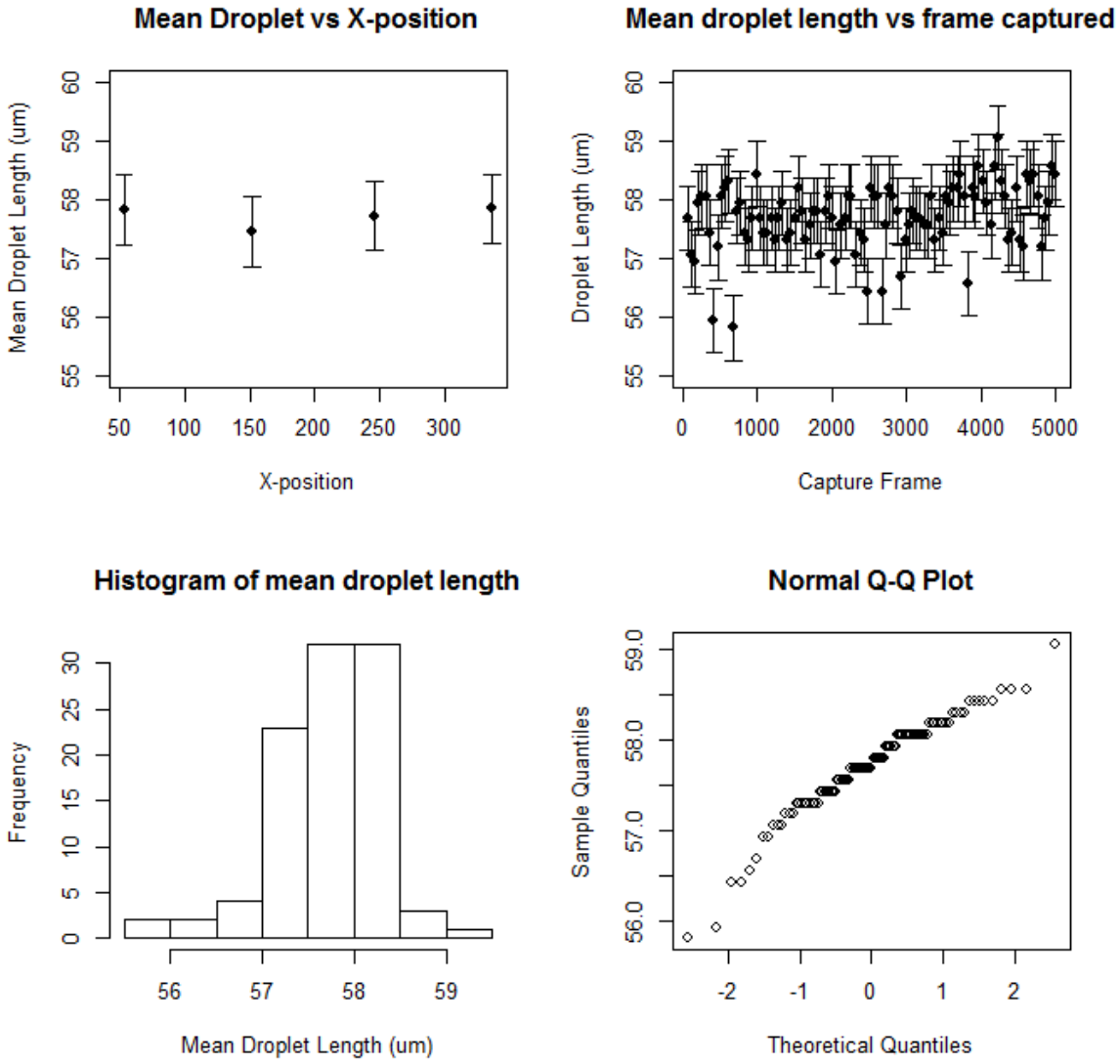

Figure 4.3: Distribution of droplet length for $P_oil = 0.1bar$

In order to investigate polydispersity of generated droplets, a large number of droplets were measured as shown in Table

$P_{OIL}(mbar)$	P_{Ratio}	Vel (m/s)	Ca	Mean Length(um)	StdDev(um)	Percent Var
20	4	0.023	0.010	57.71	0.55	0.95
40	2.25	0.033	0.014	54.53	0.35	0.64
60	1.66	0.043	0.018	48.14	0.21	0.43

4.4 Discussion

Previous work has been done to establish specific flow regimes in which droplets are formed in T-junction geometry by both numeric modeling and experimental investigations [2],[7],[8]. *However, to the best of the author's knowledge there has been no record of experimental observations demonstrating the regime transition from squeezing to dripping in a pressure-driven flow system.* This, despite the fact that there have been documented dissimilarities in volumetric versus pressure-driven flow in droplet formation[14], and that there may be advantages in droplet monodispersity in pressure-driven systems [6][10].

Previous findings suggest that two stable droplet formation regimes exist in T-junction droplet formation, *dripping* and *squeezing*. In a highly cited paper, De Menech et al showed by numerical modeling that the transition between the two distinct droplet regimes may be defined by a Critical Capillary Number, Ca_{cr}, and that this transition is independent of viscosity ratio and flowrates, shown in Figure 4.4 [7]. This transition has been previously determined both experimentally and in numerical simulations to be $Ca_{cr} \approx 10^{-2}$.

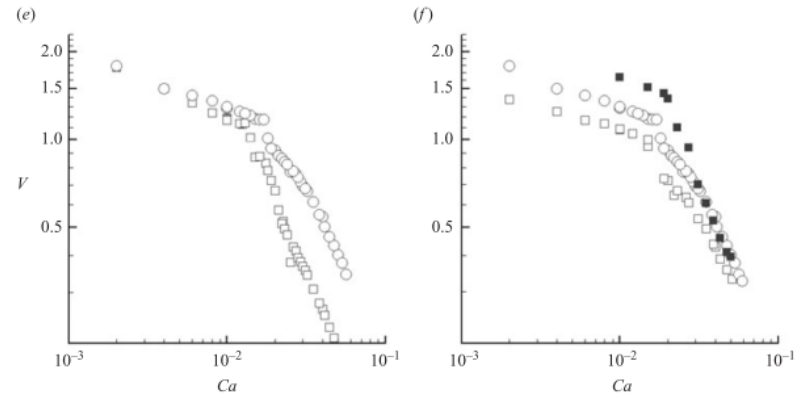

FIGURE 2. Drop formation as a function of capillary number. Two regimes of droplet formation are clearly distinguishable: at low $Ca-(a)$ $Ca=0.004$, $\lambda=1-$ and high $Ca-(b,c)$ $Ca=0.035$ and $\lambda=1/8$ and 1 respectively. At even higher Ca we observe the onset of a jet – (d) $Ca=0.05$, $\lambda=1$. (e, f) Log–log plot of droplet volume versus capillary number. (e) $Q=1/4$, and □, $\lambda=1$; ○, 1/8. (f) $\lambda=1/8$; □, $Q=1/8$; ○, 1/4; ■, 1/2. At high Ca, the droplet volume decreases more steeply, and is strongly influenced by the viscosity ratio λ.

Figure 4.4: Used directly, without permision

The data presented here shows a distinct transition between dripping and squeezing regimes, however, the Ca_{cr} value at which the transition occurs is not universal between the different continuous phase pressures. The transitional capillary number can be plotted as a function of the continuous phase pressure as shown in Figure 4.5.

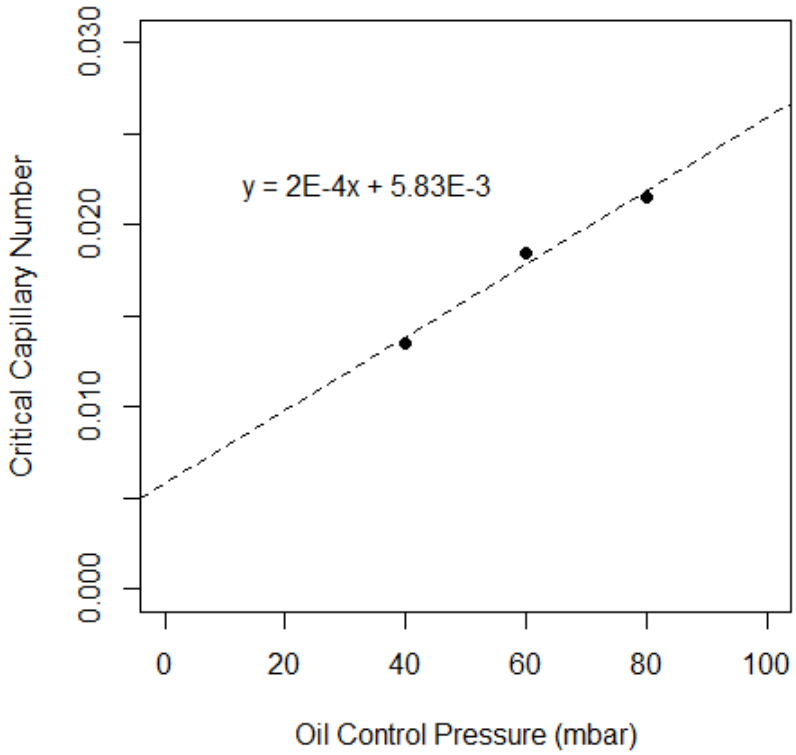

Figure 4.5: Critical capillary number as a function of continuous phase applied pressure

In these experiments the same bulk reagents are used and therefore both interfacial tension and viscosities should remain constant across multiple trials. Here, the only variable affecting variability in the Ca value is the mean velocity of the continuous phase, which in this case is approximated by direct measurement of the droplet velocity. It is expected that there is some numerical difference between the velocity of the droplets and the mean velocity of the continuous phase [14], which may account for the variability in critical capillary number.

A model of Poiseuille flow in a rectangular channel could be used to provide a more accurate determination of the mean continuous phase velocity (as a function of droplet velocity. Alternatively, due to the linear nature of relationship between applied control pressure of the continuous phase and the critical capillary number the velocities could be corrected such that the regime transition is coincident, as shown in Figure 4.6.

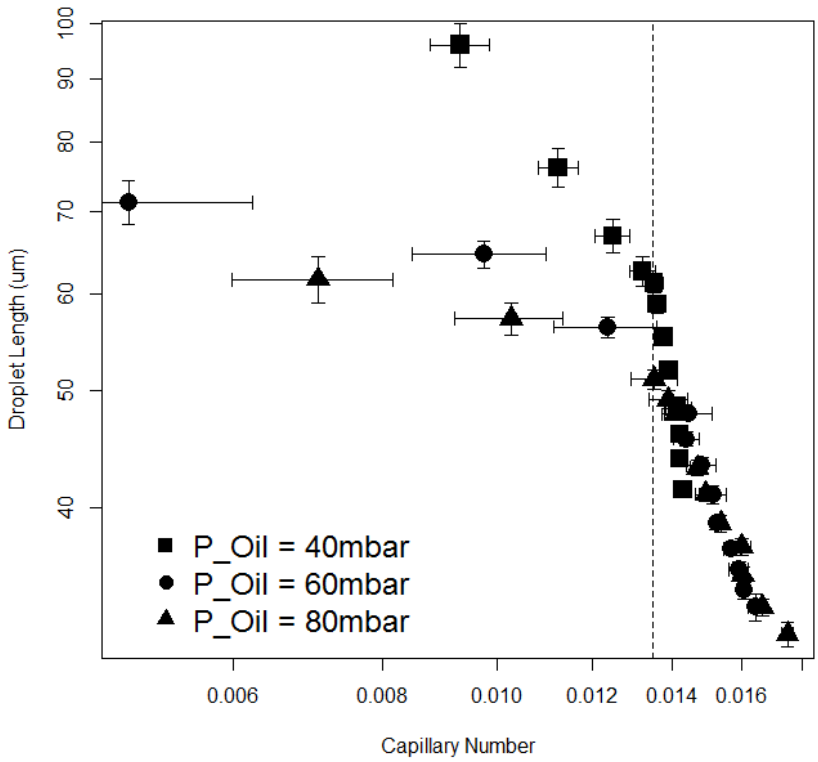

Figure 4.6: Corrected capillary number as a function of continuous phase applied pressure

In the system developed here, the only inputs used to manipulate flow behavior are the two applied pressures. Therefore, in order to characterize the system's flow regimes it is logical to determine the relationship between applied pressures and the resulting droplet velocity. Here, velocity is plotted as a function of the applied pressure ratio for both T and X-junctions as shown in Figure 4.7 on the following page. Ward determined the relationship for their system as shown in Figure 4.8 on page 20. (XX we need to do the same)

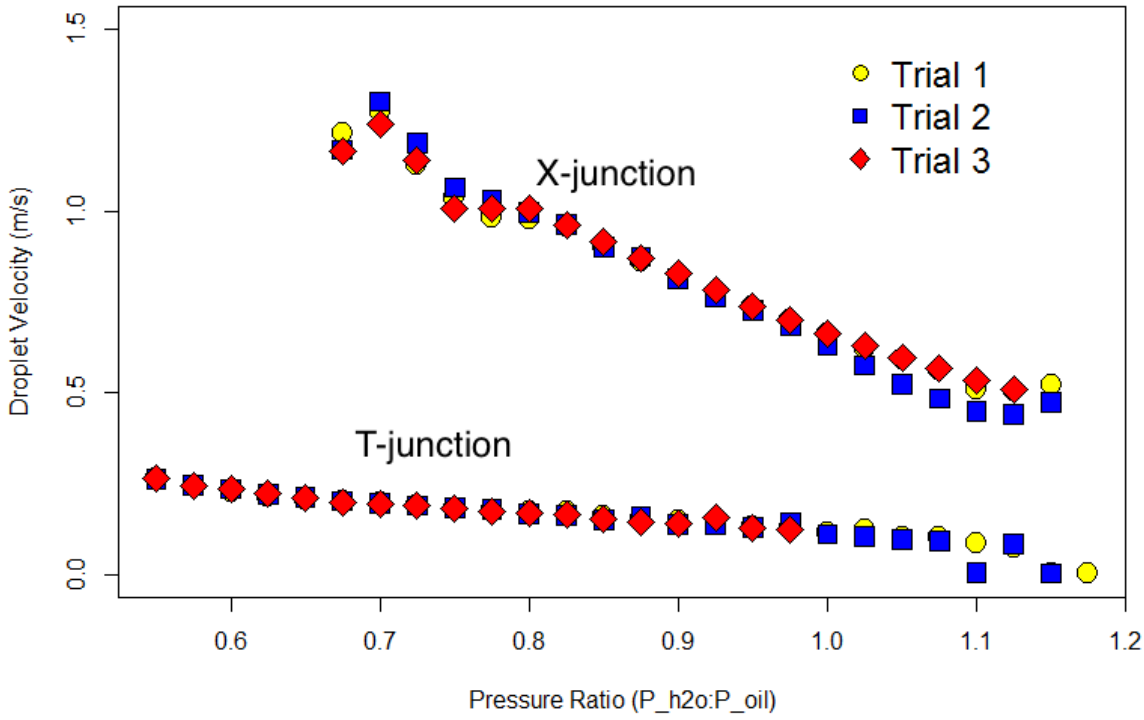

Figure 4.7: Droplet velocity for both T and X-junctions

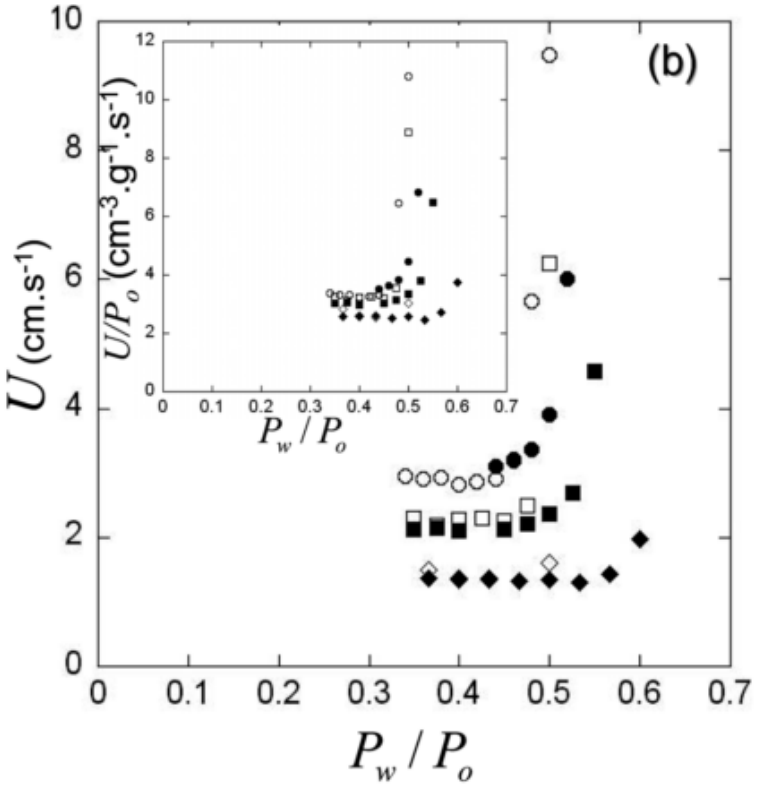

Figure 3. Measured velocity *U versus* (a) flow-rate where o, ● Q_o = 2000 μL/h, □, ■ Q_o = 1000 μL/h and (◇, ◆ Q_o = 500 μL/h and (b) inlet pressure ratio where o, ● P_o = 12.5 Psi, □, ■ P_o = 10 Psi and ◇, ◆ P_o = 7.5 Psi. The open and closed symbols are for experiments where the dispersed phase fluid flow parameter is either increased or decreased respectively.

Figure 4.8: Used without permission, taken directly from [14]

Two important observations:

1. The system used here is operating at velocities approximately a magnitude greater than Ward's system (1m/s vs 1cm/s)

2. The relationship between velocity and applied pressure ratios are different. Our system shows a relatively linear and slightly downward trending velocity while in Ward's case velocity is relatively flat then at some critical pressure increases exponentially.

From the droplet velocity Ca and Re values can be determined. Again, Ca is considerably higher than reported by others [7], [14] . A plot of droplet length versus Ca value is shown in Figure 4.9.

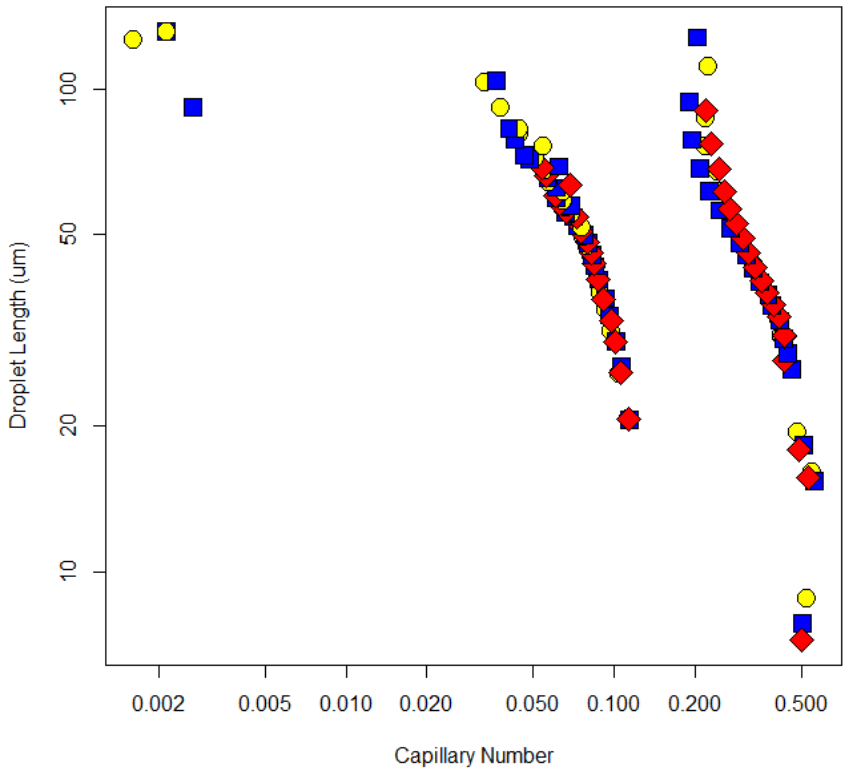

Figure 4.9: Log-Log plot Capillary Number as a function of Applied Control Pressure Ratio

Using the determined velocities Ca and Re numbers are calculated as shown in Figure **??** on page ??

	A	B	C	D	E	I	J	K	L	M
1						Velocity				
2	Note	Voil	Poil(bar)	Vh2o	Ph2o(bar)	T (m/s)	MEAN(m/s)	**Ca**	Flowrate (L/s)	**Re**
3	T-drip/noflow	2	0.4	1.1	0.22	0.266606867				
4		2	0.4	1.1	0.22	0.259131908				
5		2	0.4	1.1	0.22	0.246673643	0.257470806	**0.111242**	2.31724E-07	**10.05382**
6	Tdrip-squeeze	2	0.4	1.5	0.3	0.188119799				
7		2	0.4	1.5	0.3	0.184382319				
8		2	0.4	1.5	0.3	0.185628146	0.186043421	**0.080381**	1.67439E-07	**7.264696**
9	Tsqueeze-jet	2	0.4	2.3	0.46	0.066028804				
10		2	0.4	2.3	0.46	0.069766283				
11		2	0.4	2.3	0.46	0.068520456	0.068105181	**0.029425**	6.12947E-08	**2.659397**
12	X-drip/noflow	2	0.4	1.35	0.27	1.016594409				
13		2	0.4	1.35	0.27	1.106293915				
14		2	0.4	1.35	0.27	1.235859869	1.119582731	**0.483722**	1.00762E-06	**43.7179**
15	Xdrip-squeeze	2	0.4	1.5	0.3	1.061444162				
16		2	0.4	1.5	0.3	1.05147755				
17		2	0.4	1.5	0.3	1.05147755	1.054799754	**0.455732**	9.4932E-07	**41.18823**
18	Xsqueeze-jet	2	0.4	2.3	0.46	0.518263816				
19		2	0.4	2.3	0.46	0.518263816				
20		2	0.4	2.3	0.46	0.528230428	0.52158602	**0.225354**	4.69427E-07	**20.36709**
21										
22	**Constants**	Value	Units	Ref						
23	m/pixel	4.98E-07								
24	Oil Visc	0.00124	Pa-s@25d(	DataSheet						
25	Oil Density	1614	Ns^2/m^4							
26	Interfacial Tensio	0.00287	N/m	unknown						
27	Channel Area	9E-10	m^2							
28	Channel width	0.00003	m^2							

Figure 4.10: Re Ca Calculations

In order to qualitatively characterize the formation of droplets across the entire range of functional pressure ratios, the following section will describe the system behavior at the states of no-flow, dripping, squeezing, and jetting. Due to the strong similarities in droplet-formation behavior between the X-junction and T-junction geometry they will be discussed in general terms with specific metrics given for each case.

No-Flow As the system is moved towards the lowest operational pressure ratios, the aqueous phase comes to a a quasi equilibrium no-flow state. As previously reported by Ward et al citeWard2005 . If the pressure ratio is decreased any further(either by increasing P_{Oil} or decreasing P_{H_2O}) back-flow will occur, in which the continuous phase begins displacing the aqueous phase upstream towards the reservoir. This quasi equilibrium state may be described as a balance of forces between the pressure of the two phases and the Laplace pressure differential across the liquid-liquid interface, described as shown in Equation 4.2.

$$P_{H_2O*} + P_{Laplace} = P_{Oil*} \tag{4.2}$$

Where Laplace pressure can be roughly approximated given γ is the interfacial tension between the two phases, r is the radius of curvature of the interface as:

$$P_{Laplace} = \frac{2\gamma}{r} \tag{4.3}$$

It should be noted that here P_{H_2O*} and P_{Oil*} represent the pressures of the two phases local to the X or T junction and that there is some unknown pressure drop between the applied control pressures at the inlet reservoirs and these local pressures. This pressure drop is dependent on device geometry as well as solution viscosity and can be determined by Hagan-Poiseuille approximations (XX - needs to be done).

Dripping As the control pressure applied to the discontinuous phase is increased beyond the *no-flow* state the immiscible thread begins to extend into the device's channel junction.

Squeezing The pinch point moving further downstream is a manifestation of the increases in tangental viscous forces relative to inertial forces (Ca). The Ca value increases due to the increase in velocity as the interfacial tension and viscosity are both constant. The viscous forces acting tangentially to the discontinuous phase

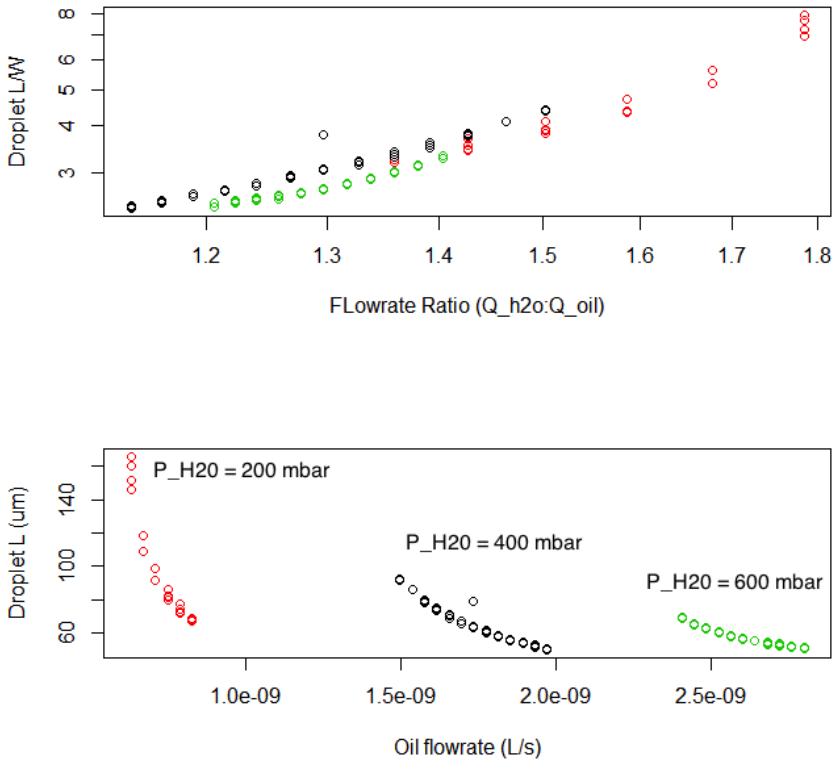

Figure 4.11: Droplet length at varying flowrates

boundary elongates the immiscible thread before the combined effect of increased plugging pressure and inertial forces finally dominate leading to droplet formation.

Chapter 5

Conclusions

Appendix A

Arduino Code

```
//Aaron Delahanty
//2224135D@student.gla.ac.uk
//University of Glasgow
//21Oct2015
//Electronic Flow Controller

//This application (sketch) is intended to be the sole sketch responsible for
    measuring
//and regulating pressure in the Electronic Flow Control (EFC) system being developed
//for T.Franke's microfluidic group. The objective of the sketch is to faciliate
//communication with two types of integrated chips (i) Analog Microselectronic's
    AMS5915
//pressure sensors,and (ii) Microchip Technology Inc.'s MCP4921 DAC.

//In addition to this sketch the system will use a LabView VI to set the desired
//pressure values by DAC, and display the measured pressure for the 4 discrete
    channels
//This communication will be facilated by serial communication over USB.

//Revision Notes:
//02192016  - Removed Volmeter functionality
//          - Removed All Delays
//          - 4th Channel DAC is faulting (output is always 1V)


//Wire.h is the arduino library for I2C/TWI comm
#include <Wire.h>
#include <SPI.h>

//Define variables used for conversion of pressure units from raw counts mbar.
    int p_min;
    int p_max;
    int digoutp_min;
    int digoutp_max;

//Define array for pressure channel comaprison and final output
//Comparison is used to determine whether the high range 1000mbar or high resolution
//350mbar sensor should be used
    float p_comp[8];
    float p_out[4];

//Prior to sending the 12bit input which will drive the T2000 pressure regulators
//the DAC needs to receive 4 configuration bits
//Bit 15 - 0 = write to DAC, 1 = ignore command
//Bit 14 - BUF; 1 = buffer v_ref, 0 = bypass buffer
//Bit 13 - GA; 1 = v_out is 1X v_ref, 0 = vout is 2X v_ref
```

```
//Bit 12 - SHDN; 1 = active, 0 = shutdown DAC

//Default configuration bits set to [0,1,1,1]
    unsigned int Config = B0111;

void setup()
{
    //Set baud rate to 9600
    Serial.begin(9600);
    // join i2c bus
    Wire.begin();
    // join SPI bus
    SPI.begin();
}

void loop()
{

//START DAC CODE:

 // check serial

  if ( Serial.available() ){
    // cast the string read in an integer
    String p_write = Serial.readString();

  int commaIndex1 = p_write.indexOf(',');
  int commaIndex2 = p_write.indexOf(',',commaIndex1+1);
  int commaIndex3 = p_write.indexOf(',',commaIndex2+1);


  String P1s = p_write.substring(0,commaIndex1);
  String P2s = p_write.substring(commaIndex1+1,commaIndex2);
  String P3s = p_write.substring(commaIndex2+1,commaIndex3);
  String P4s = p_write.substring(commaIndex3+1);

  unsigned int a[3];
  a[0]=P1s.toInt();
  a[1]=P2s.toInt();
  a[2]=P3s.toInt();
  a[3]=P4s.toInt();


    float cs[3];
    for (int i = 0; i <= 3; i++)
       {
        cs[i] = i+7;
        pinMode(cs[i], OUTPUT);



        //Command is the variable sent to DAC to drive pressure regulator
        //The commmand variable is comprised of the 4 configuration bits and 12 data
            bits
        unsigned int command;
        //Shift the config bits 12 positions leftward, augment with the a[i] pressure
             value
        //in volts
        command = ( Config << 12 | a[i]);

        //Write command to each ith DAQ
        SPI.beginTransaction(SPISettings(20000000, MSBFIRST, SPI_MODE0));
        //Set ith output pin to LOW, in order to accept write command
        digitalWrite(cs[i], LOW);
        //SPI.transfer function is only capable of sending 8bits at a time
        //The 16bit command is therefore split into a high and low byte
        int high = highByte(command);
        int low = lowByte(command);
```

```
        SPI.transfer(high);
        SPI.transfer(low);
        SPI.endTransaction();
        //Set ith pin HIGH to end write command
        digitalWrite(cs[i], HIGH);
        //Optional print for debugging
        //Serial.println("16bit command sent:");
        //Serial.println(value,BIN);
        }
  }


//END DAC CODE

//START PRESSURE SENSOR CODE:

  //Define buffer to hold sampled values
  byte buffer[4];


  for (int addr = 1; addr <= 8; addr++)
    {
        //Pressure sensor addresses have been configured to 1 through 8.
        //Sensors 1,2,3,4 are high range 1000mbar
        if (addr <= 4)
          {
            //Set conversion constants for AMS 5915-1000-D
            p_min = 0;
            p_max = 1000;
            digoutp_min = 1638;
            digoutp_max = 14745;
          }

        //Sensors 5,6,7,8 are high resolution 350mbar
        else
          {
            //Set conversion constants for AMS 5915-350-D-B
            p_min = 0;
            p_max = 350;
            digoutp_min = 1638;
            digoutp_max = 14745;
          }

        //Wire.requestFrom(address, quantity)
        //address: the 7-bit address of the device to request bytes from
        //quantity: the number of bytes to request
        //request four bytes from sensor (first 2 are pressure, second 2 are temp)
        int n = Wire.requestFrom (addr, 4);

        //Ensure response is 4byte
        if(n == 4)
          {

            Wire.readBytes (buffer, 4);

            unsigned int p_raw = word (buffer[0], buffer[1]);     // word(high,low)
            unsigned int t_raw = word (buffer[2], buffer[3]);

            // note that the next bit operations works best with "unsigned int", not
                with "int"
            p_raw &= 0x3FFF;    // 14bits pressure data
            t_raw >>= 5 ;       // 11bits temeperature data, shift them in position


            // convert raw pressure to mbar (equation and constants from datasheet)
            float pressure = ((( (float) p_raw - digoutp_min ) / ((digoutp_max -
                digoutp_min) / (p_max - p_min ))) + p_min );
```

```
            // convert raw temperature to degC (equation and constants from datasheet
                )
            float temperature = (( (float) t_raw * 200.0 ) / 2048.0 ) - 50.0;

            // with the pressure comparison array with all sensor's outputs
            p_comp[addr-1] = pressure;
          }

        //If no response is present, or response is not 4bytes
        else
          {
          Serial.println ("Error, no sensor found");
          }
    }


   int i;
   for (i = 0; i <= 3; i++)
     {
        if (p_comp[i]> 350)
          {
            p_out[i] = p_comp[i];
          }
        else
          {
           p_out[i] = p_comp[i+4];
          }
        Serial.println(p_out[i]);
     }
// END PRESSURE SENSOR CODE

}
```

Appendix B

LabVIEW VI

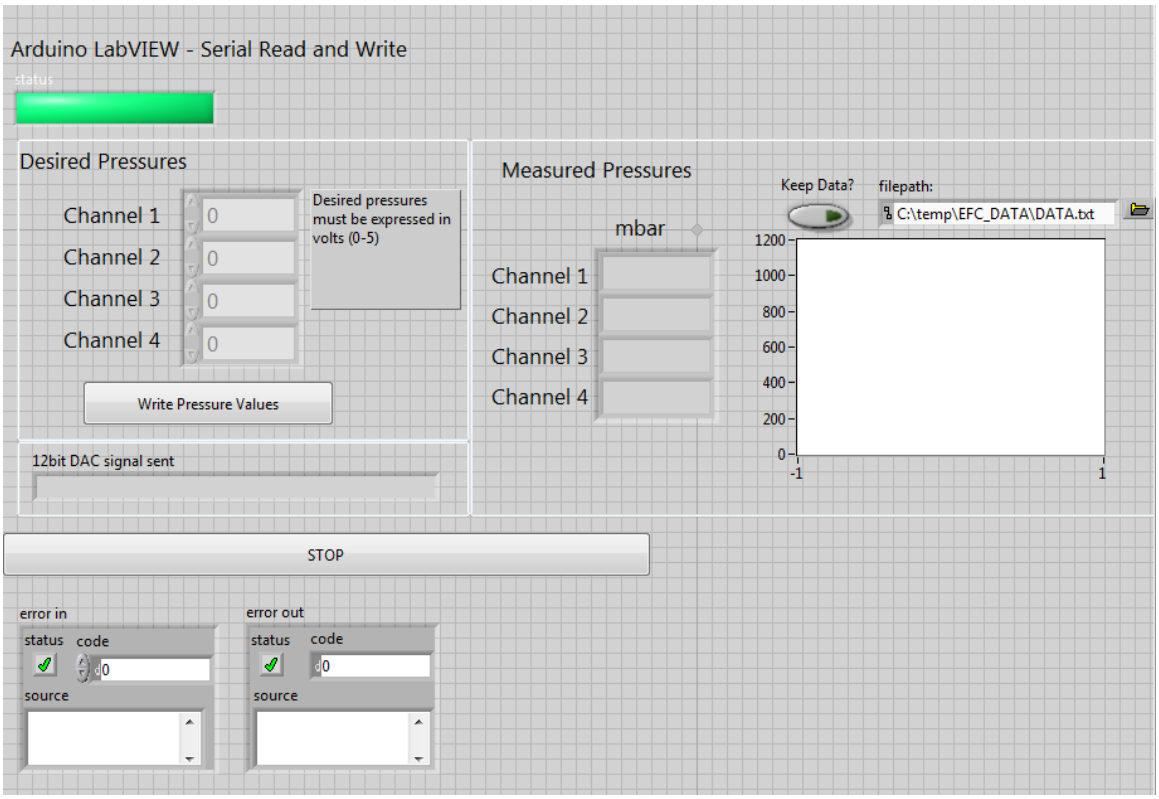

Figure B.1: LabVIEW Frontend

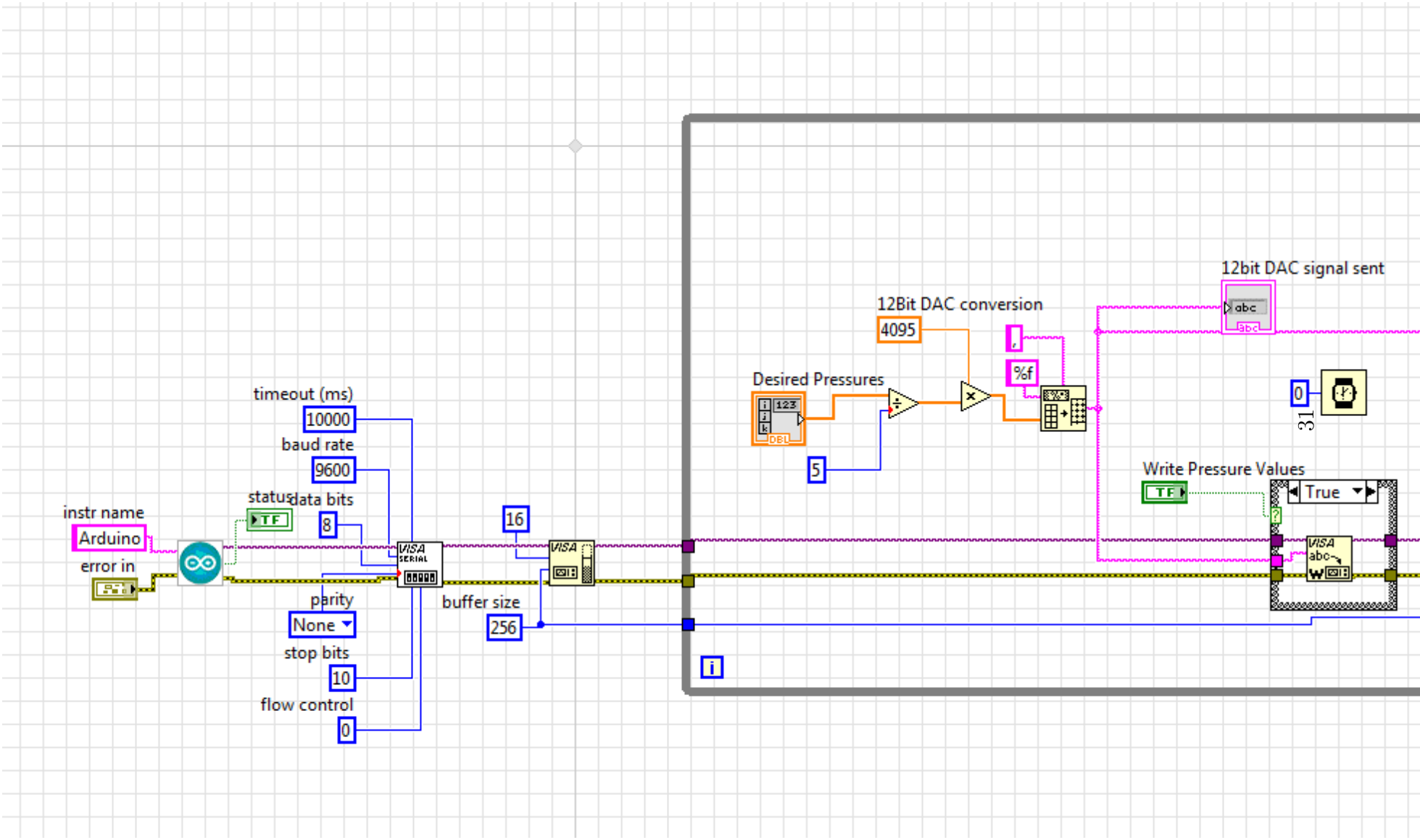
instr name
Arduino
error in
status
TF
timeout (ms)
10000
baud rate
9600
data bits
8
parity
None
stop bits
10
flow control
0
VISA SERIAL
16
VISA
buffer size
256
Desired Pressures
123
DBL
5
12Bit DAC conversion
4095
%f
12bit DAC signal sent
abc
0
31
Write Pressure Values
TF
True
VISA
abc
i

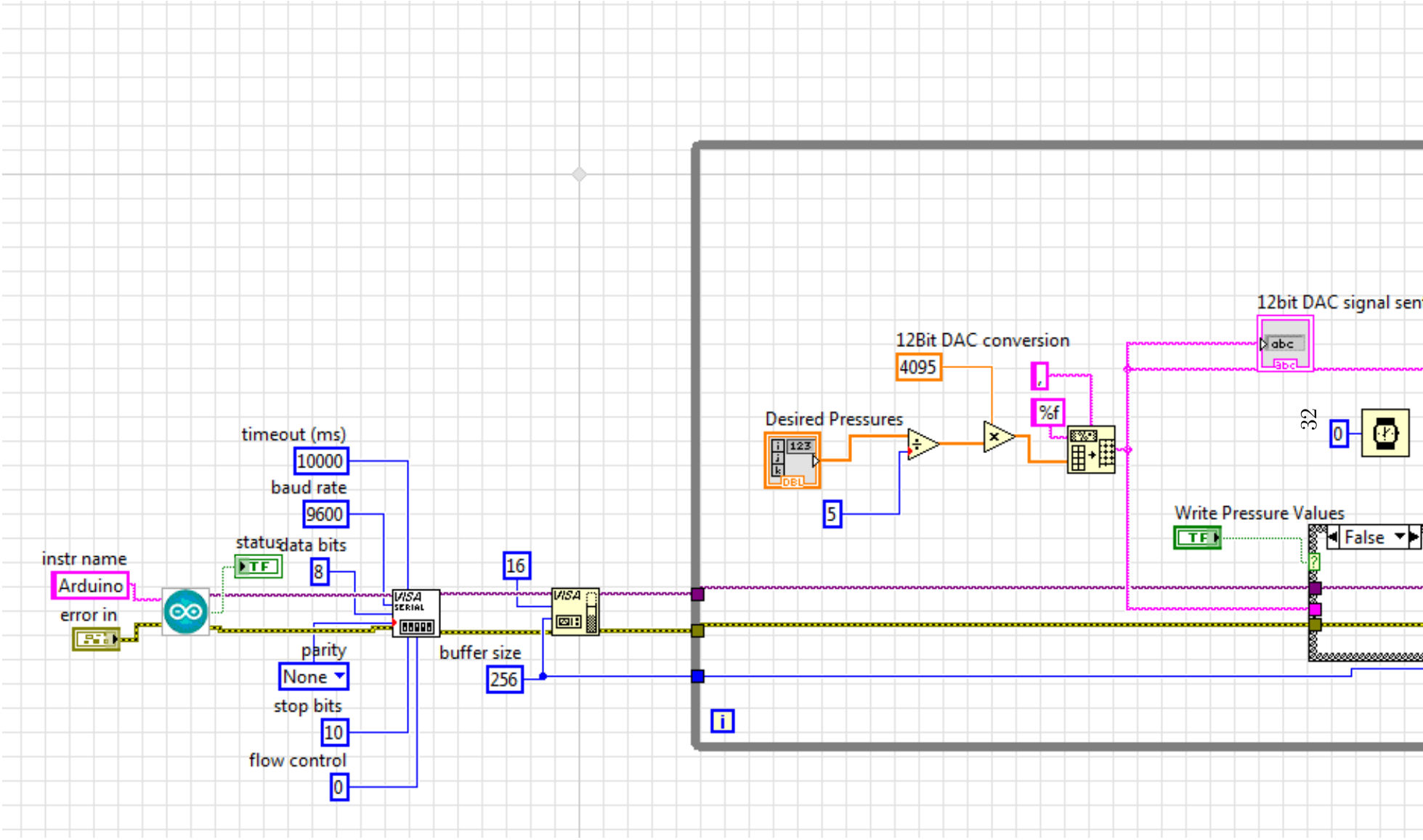
timeout (ms)
10000
baud rate
9600
status
data bits
8
instr name
Arduino
error in
parity
None
stop bits
10
flow control
0
16
buffer size
256
12Bit DAC conversion
4095
Desired Pressures
5
%f
12bit DAC signal sent
0
Write Pressure Values
False

Bibliography

[1] 3M. 3M Novec 7200 Engineered Fluid. Datasheet, 2009.

[2] Adam R. Abate, Pascaline Mary, Volkert van Steijn, and David A. Weitz. Experimental validation of plugging during drop formation in a T-junction. *Lab on a Chip*, 12(8):1516, 2012.

[3] Henrik Bruus. *Theoretical Microfluidics*. Oxford ; New York : Oxford University Press, 2008., 2008.

[4] Lorenzo Capretto, Wei Cheng, Martyn Hill, and Xunli Zhang. Micromixing within microfluidic devices. *Topics in Current Chemistry*, 304(1):27–68, 2011.

[5] Zhuang Zhi Chong, Say Hwa Tan, Alfonso M Ganan-Calvo, Shu Beng Tor, Ngiap Hiang Loh, and Nam-Trung Nguyen. Active droplet generation in microfluidics. *Lab Chip*, 16:35–58, 2016.

[6] Gordon F. Christopher, N. Nadia Noharuddin, Joshua A. Taylor, and Shelley L. Anna. Experimental observations of the squeezing-to-dripping transition in T-shaped microfluidic junctions. *Physical Review E - Statistical, Nonlinear, and Soft Matter Physics*, 78(3), 2008.

[7] M. De Menech, P. Garstecki, F. Jousse, and H. a. Stone. Transition from squeezing to dripping in a microfluidic T-shaped junction. *Journal of Fluid Mechanics*, 595:141–161, 2008.

[8] Piotr Garstecki, Michael J. Fuerstman, Howard A. Stone, and George M. Whitesides. Formation of droplets and bubbles in a microfluidic T-junctionscaling and mechanism of break-up. *Lab on a Chip*, 6(3):437, 2006.

[9] Clement Kleinstreuer. *Microfluidics and Nanofluidics: Theory and Selected Applications: Theory and Selected Applications*. 2013.

[10] Zida Li, Sze Yi Mak, Alban Sauret, and Ho Cheung Shum. Syringe-pump-induced fluctuation in all-aqueous microfluidic system implications for flow rate accuracy. *Lab on a Chip*, 14(4):744, 2014.

[11] Princeton Microfluidics. Microfluidics Bootcamp 2014. 2014.

[12] Lingling Shui, J. C T Eijkel, and Albert van den Berg. Multiphase flow in micro- and nanochannels. *Sensors and Actuators, B: Chemical*, 121(1):263–276, 2007.

[13] Lingling Shui, Jan C T Eijkel, and Albert van den Berg. Multiphase flow in microfluidic systems - Control and applications of droplets and interfaces. *Advances in Colloid and Interface Science*, 133(1):35–49, 2007.

[14] Thomas Ward, Magalie Faivre, Manouk Abkarian, and Howard A. Stone. Microfluidic flow focusing: Drop size and scaling in pressure versus flow-rate-driven pumping. *Electrophoresis*, 26(19):3716–3724, 2005.

[15] Chun Guang Yang, Zhang Run Xu, and Jian Hua Wang. Manipulation of droplets in microfluidic systems. *TrAC - Trends in Analytical Chemistry*, 29(2):141–157, 2010.

[16] Chun Xia Zhao and Anton P J Middelberg. Two-phase microfluidic flows. *Chemical Engineering Science*, 66(7):1394–1411, 2011.